Computer Assisted Mechanics and Engineering Sciences, 8: 235–246, 2001.

Hybrid-Trefftz stress elements for three-dimensional elastoplasticity

Flávio L.S. Bussamra
Agrupamento de Estruturas, Instituto de Pesquisas Tecnológicas do Estado de São Paulo, São Paulo, Brasil

Paulo de Mattos Pimenta
Departamento de Engenharia de Estruturas e Fundações, Escola Politécnica da Universidade de São Paulo, São Paulo, Brasil

João A. Teixeira de Freitas
Departamento de Engenharia Civil e Arquitectura, Instituto Superior Técnico, Universidade Técnica de Lisboa, Lisboa, Portugal

(Received June 30, 2000)

The stress model of the hybrid-Trefftz finite element formulation is applied to the elastoplastic analysis of solids. The stresses and the plastic multipliers in the domain of the element and the displacements on its boundary are approximated. Harmonic and orthogonal hierarchical polynomials are used to approximate the stresses, constrained to solve locally the Beltrami governing differential equation. They are derived from the associated Papkovitch-Neuber elastic displacement solution. The plastic multipliers are approximated by Dirac functions defined at Gauss points. The finite element equations are derived directly from the structural conditions of equilibrium, compatibility and elastoplasticity. The non-linear governing system is solved by the Newton method. The resulting Hessian matrices are symmetric and highly sparse. All the intervening arrays are defined by boundary integral expressions or by direct collocation. Numerical applications are presented to illustrate the performance of the model.

1. Introduction

The paper reports on the application of the hybrid-Trefftz stress finite element to the elastoplastic analysis of solids. It shown in [4, 7] that this element performs rather well when applied to the solution of elastic three-dimensional benchmark problems. It exhibits a negligible sensitivity to geometric irregularities and to gross mesh distortion, it is free from locking in the incompressibility or near incompressibility limit and produces accurate estimates for both stresses and displacements.

The non-linear application reported has been selected to assess the combination of the high levels of performance that can be attained with three-dimensional hybrid-Trefftz finite elements with the robustness and proven reliability of the implicit Euler backward stress integration and the Newton-Raphson method, as applied to the elastoplastic analysis of solids, e.g. [8, 9].

The formulation is based on the independent approximation of three fields. Stresses and plastic multipliers are approximated in the domain of the element and the displacements are approximated independently on its static (Neumann) boundary. A polynomial basis for the stress field is derived from the Papkovitch–Neuber potential that solves locally the homogeneous Navier equation. This polynomial basis is free of spurious modes and involves 186 degrees of freedom for a complete sixth-degree stress approximation.

The resulting Hessian matrices are symmetric and highly sparse. All intervening matrices and vectors are either defined by boundary integral expressions, which is typical of the Trefftz approach, or computed from direct collocation, as a result of the Dirac approximation of the plastic multiplier field.

The tests presented here for the elastoplastic analysis of solids confirm the high efficiency that can be attained in the solution of both linear and non-linear problems reported in [10,12–17] two-dimensional applications.

2. Fundamental relations

Let V and Γ denote the domain and the boundary of a typical finite element and let Γ_u and Γ_σ identify the kinematic (Dirichlet) and static (Neumann) boundaries: $\Gamma = \Gamma_u \cup \Gamma_\sigma$; $\emptyset = \Gamma_u \cap \Gamma_\sigma$.

In the equilibrium and compatibility conditions (1) to (4), $\boldsymbol{u}$ is the displacement vector and vectors $\boldsymbol{\sigma}$ and $\boldsymbol{\varepsilon}$ collect the independent components of stress and strain tensors, respectively,

$$\boldsymbol{D\sigma} = \boldsymbol{0} \qquad \text{in } V, \tag{1}$$

$$\boldsymbol{\varepsilon} = \boldsymbol{D}^* \boldsymbol{u} \qquad \text{in } V, \tag{2}$$

$$\boldsymbol{N\sigma} = \boldsymbol{t}_\Gamma \qquad \text{on } \Gamma_\sigma , \tag{3}$$

$$\boldsymbol{u} = \boldsymbol{u}_\Gamma \qquad \text{on } \Gamma_u . \tag{4}$$

For simplicity, the body forces are neglected in the domain equilibrium condition (1), where $\boldsymbol{D}$ is the differential equilibrium operator. In the domain compatibility condition (2), $\boldsymbol{D}^*$ is the adjoint operator for geometrically linear problems. In the Neumann condition (3), $\boldsymbol{N}$ is the boundary equilibrium matrix that collects components of the unit outward normal vector to Γ and $\boldsymbol{t}_\Gamma$ is the prescribed traction vector. In the Dirichlet condition (4), vector $\boldsymbol{u}_\Gamma$ defines the prescribed displacements.

The decomposition of the strains into elastic and plastic addends is defined by Eqs. (5) and (6) states the elasticity condition in terms of the flexibility matrix, $\boldsymbol{f}$,

$$\boldsymbol{\varepsilon} = \boldsymbol{\varepsilon}_e + \boldsymbol{\varepsilon}_p \qquad \text{in } V, \tag{5}$$

$$\boldsymbol{\varepsilon}_e = \boldsymbol{f\sigma} \qquad \text{in } V. \tag{6}$$

In the perfect plasticity equations (7)–(10), $F(\boldsymbol{\sigma})$ is the yield function, λ is the plastic multiplier, and $\boldsymbol{n}(\boldsymbol{\sigma})$ is the outward normal vector to the yield surface and $F(\boldsymbol{\sigma}) = 0$.

$$F(\boldsymbol{\sigma}) \leq 0 \qquad \text{in } V, \tag{7}$$

$$\dot{\boldsymbol{\varepsilon}}_p = \dot{\lambda} \boldsymbol{n}(\boldsymbol{\sigma}) \qquad \text{in } V, \tag{8}$$

$$\boldsymbol{n}(\boldsymbol{\sigma}) = \frac{\partial F(\boldsymbol{\sigma})}{\partial \boldsymbol{\sigma}} \qquad \text{in } V, \tag{9}$$

$$\dot{\lambda} \geq 0 \qquad \text{in } V. \tag{10}$$

3. Finite element aproximations

The hybrid finite element formulation used here is based on the direct approximation of the stresses and plastic multiplier increments in the domain of the element and, also, of the displacements on its Neumann boundary,

$$\boldsymbol{\sigma} = \boldsymbol{SX} \qquad \text{in } V, \tag{11}$$

$$\Delta\lambda = \boldsymbol{E}_* \boldsymbol{e}_* \qquad \text{in } V, \tag{12}$$

$$\boldsymbol{u} = \boldsymbol{Zq} \qquad \text{on } \Gamma_\sigma . \tag{13}$$

In the definitions above, $\boldsymbol{S}$, $\boldsymbol{E}_*$ and $\boldsymbol{Z}$ are the matrices that collect the approximation functions. As generalised (non-nodal) variables are used, the weighting vectors $\boldsymbol{X}$, $\boldsymbol{e}_*$ and $\boldsymbol{q}$ define generalised stresses, plastic multipliers and boundary displacements, respectively.

Neither the formulation nor the approximation bases used here constrain the geometry of the finite element, which may not be convex, bounded or simply connected. However, and for simplicity, only one master element is tested in this report, namely the right 8-node hexahedron. The shape functions adopted in the mapping operations typical of isoparametric elements are used here only to support the geometric transformations, as the finite element approximation is implemented on the independent bases defined below.

3.1. Stress approximation

In the Papkovitch–Neuber solution (14) of the (elastic, homogeneous) Navier equation, G is the shear modulus, ν is the Poisson ratio, $\boldsymbol{r}$ and $\boldsymbol{\nabla}$ are the position and gradient vectors and operators $\boldsymbol{\psi}$ and ϕ are vector and scalar harmonic displacement potentials, respectively,

$$2G\boldsymbol{U} = -4(1-\nu)\boldsymbol{\psi} + \boldsymbol{\nabla}(\boldsymbol{r}^t\boldsymbol{\psi} + \phi). \tag{14}$$

This solution is used to establish the stress approximation matrix. Equations (2) and (6) yield the following expression, where $\boldsymbol{k} = \boldsymbol{f}^{-1}$,

$$\boldsymbol{S} = \boldsymbol{k}\boldsymbol{D}^*\boldsymbol{U}. \tag{15}$$

The following displacement potentials are used to build this basis,

$$\varphi_k^L = r^n P_n(\xi_k), \tag{16}$$

$$\phi_k = r_k^n \exp(\theta_k), \tag{17}$$

$$\varphi_k = x_k r_k^n \exp(\theta_k). \tag{18}$$

In the definitions above, P_n is the associated Legendre function of order n, $r = \sqrt{x_1^2 + x_2^2 + x_3^2}$, $r_k = \sqrt{x_i^2 + x_j^2}$, $\theta_k I \tan^{-1}(x_j/x_i)$, I is the imaginary unit, $\xi_k = x_k/r$ and x_k represents the local (baricentric) system of co-ordinates assigned to the element.

When n is integer and an even permutation of i, j and k is used, the real and imaginary parts of definitions (16) to (18) define polynomial potential functions [7]. The fifteen functions thus defined are inserted in Eqs. (14) and (15) to generate sixty polynomial approximation functions for each degree, n. Although it is complete, this Papkovitch–Neuber basis may contain linearly dependent modes, which are detected and eliminated from the stress basis (15) *a priori*.

As it shown in [7], the stress basis generated in this manner is self-equilibrated, and described by 186 complete, linearly independent polynomial stress modes of the sixth degree. Higher degree bases are possible, but complete extensions are yet to generated. For Instance, the potential functions (16) to (18) generate stress basis with completeness deficits of 6, 16 and 31 modes for the known totals of 237, 294 and 357 independent modes present in complete bases of degree seven, eight and nine, respectively.

3.2. Boundary displacements approximation

The approximation matrix, Z, present in the boundary displacement approximation (13) is built on a complete, linearly independent and naturally polynomial bases directly extracted from the Pascal triangle [7]. This basis is written in the local co-ordinate system assigned to each face of the master element. The number of boundary displacement modes that are thus generated for a complete basis of degree n is defined by

$$n_z = 3\,[1/2(n+1)(n+2)]\,. \tag{19}$$

3.3. Plastic multiplier approximation

The plastic multiplier increment in definition (11) is approximated by Dirac functions $\hat{\delta}(x)$. Preliminary tests have shown that, as expected, the Gauss integration points provide the best choice for the control of plastic deformation [4]. Therefore, the plastic multiplier approximation matrix and the associated plastic multipliers vector are defined as follows, where $\boldsymbol{x}_1$, $\boldsymbol{x}_2$, ..., $\boldsymbol{x}_N$ denote the Gauss points,

$$\boldsymbol{E}_* = \left[\hat{\delta}(\boldsymbol{x}_1),\ \hat{\delta}(\boldsymbol{x}_2),\ \ldots \hat{\delta}(\boldsymbol{x}_N)\right], \tag{20}$$

$$\boldsymbol{e}_* = [\Delta\lambda(\boldsymbol{x}_1)\quad \Delta\lambda(\boldsymbol{x}_2)\quad \ldots\quad \Delta\lambda(\boldsymbol{x}_N)]^t. \tag{21}$$

4. Finite element equations

Different approaches can be followed to establish the finite element equations resulting from the basic approximations (11) to (13), namely duality, virtual work and variational approaches.

For instance, the weak form (22) of the virtual work equation can be used to derive Eq. (23), which enforces on average, in the sense of Galerkin, the compatibility conditions (2) and (4) and the elasticity condition (6) for decomposition (5),

$$\int_V \delta\boldsymbol{\sigma}^t\boldsymbol{\varepsilon}\,\mathrm{d}V = \int_{\Gamma_\sigma} (\boldsymbol{N}\delta\boldsymbol{\sigma})^t\boldsymbol{u}\,\mathrm{d}\Gamma + \int_{\Gamma_u} (\boldsymbol{N}\delta\boldsymbol{\sigma})^t\boldsymbol{u}_\Gamma\,\mathrm{d}\Gamma, \tag{22}$$

$$\boldsymbol{F}\boldsymbol{X} - \boldsymbol{A}\boldsymbol{q} + \int_V \boldsymbol{S}^t\boldsymbol{\varepsilon}_p\,\mathrm{d}V = \boldsymbol{v}. \tag{23}$$

In the equation above, $\boldsymbol{F}$ and $\boldsymbol{A}$ are the finite element flexibility and compatibility matrices, respectively, and vector $\boldsymbol{v}$ defines the contribution of the prescribed displacements,

$$\boldsymbol{F} = \int_V \boldsymbol{S}^t\boldsymbol{f}\boldsymbol{S}\,dV, \tag{24}$$

$$\boldsymbol{A} = \int_{\Gamma_\sigma} (\boldsymbol{N}\boldsymbol{S})^t\boldsymbol{Z}\,\mathrm{d}\Gamma, \tag{25}$$

$$\boldsymbol{v} = \int_{\Gamma_u} (\boldsymbol{N}\boldsymbol{S})^t\boldsymbol{u}_\Gamma\,\mathrm{d}\Gamma. \tag{26}$$

Additionally, the weak form (27) of the Neumann equilibrium condition (3) leads to the ($\boldsymbol{Z}$-weighted, Galerkin) finite element description (28), where vector $\boldsymbol{Q}$ defines the contribution of the prescribed tractions,

$$\int_{\Gamma_\sigma} \delta\boldsymbol{u}^t\boldsymbol{N}\boldsymbol{\sigma}\,\mathrm{d}\Gamma = \int_{\Gamma_\sigma} \delta\boldsymbol{u}^t\boldsymbol{t}_\Gamma\,\mathrm{d}\Gamma, \tag{27}$$

$$-\boldsymbol{A}^t\boldsymbol{X} = -\boldsymbol{Q}, \tag{28}$$

$$\boldsymbol{Q} = \int_{\Gamma_\sigma} \boldsymbol{Z}^t\boldsymbol{t}_\Gamma\,\mathrm{d}\Gamma. \tag{29}$$

It is noted that the domain equilibrium condition (1) is locally satisfied by the self-equilibrated stress approximation (11), $\boldsymbol{D}\boldsymbol{S} = \boldsymbol{0}$. This property, together with condition (15), can be used to obtain the following boundary integral definition for the finite element flexibility matrix (24) [7], as it is typical of the Trefftz variant of the finite element method,

$$\boldsymbol{F} = \int_\Gamma (\boldsymbol{N}\boldsymbol{S})^t\boldsymbol{u}\,\mathrm{d}\Gamma. \tag{30}$$

4.1. Time discretisation of the plastic strain

It is assumed that the loading programme is applied in N time steps $[t_i\,,\,t_{i+1}]$. The response of the structure is fully determined at instant t_i and at instant t_{i+1} either the loads or the displacements applied to the structure are prescribed. The following non-linear system is obtained combining, at instant t_{i+1}, Eqs. (23) and (28) and the plastic yield condition (7),

$$\boldsymbol{F}\boldsymbol{X}_{i+1} - \boldsymbol{A}\boldsymbol{q}_{i+1} + \int_V \boldsymbol{S}^t \boldsymbol{\varepsilon}_{p_{i+1}}\,\mathrm{d}V = \boldsymbol{v}_{i+1}\,, \tag{31a}$$

$$-\boldsymbol{A}^t\boldsymbol{X}_{i+1} = -\boldsymbol{Q}_{i+1}\,, \tag{31b}$$

$$F(\boldsymbol{\sigma}_{i+1}) \le 0. \tag{31c}$$

The plastic strain increment in time step $[t_i, t_{i+1}]$ is given as follows, where $\boldsymbol{\varepsilon}_{p_{i+1}} = \boldsymbol{\varepsilon}_{p_i} + \Delta\boldsymbol{\varepsilon}_p$,

$$\Delta\boldsymbol{\varepsilon}_p = \int_{t_i}^{t_{i+1}} \dot{\boldsymbol{\varepsilon}}_p\,\mathrm{d}t = \int_{t_i}^{t_{i+1}} \dot{\lambda}\boldsymbol{n}\,\mathrm{d}t\,. \tag{32}$$

The implicit backward Euler integration of the above relation leads to definition $\boldsymbol{\varepsilon}_{p_{i+1}} = \boldsymbol{\varepsilon}_{p_i} + \Delta\lambda\boldsymbol{n}_{i+1}$, which is enforced in Eq. (31a) to yield

$$\boldsymbol{F}\boldsymbol{X}_{i+1} - \boldsymbol{A}\boldsymbol{q}_{i+1} + \int_V \boldsymbol{S}^t\boldsymbol{n}_{i+1}\Delta\lambda\,\mathrm{d}V = \boldsymbol{v}_{i+1} - \boldsymbol{e}_{p_i}\,, \tag{33}$$

$$\boldsymbol{e}_{p_i} = \int_V \boldsymbol{S}^t\boldsymbol{\varepsilon}_{p_i}\,\mathrm{d}V. \tag{34}$$

The following results are obtained combining Eqs. (12), (20) and (33),

$$\int_V \boldsymbol{S}^t\boldsymbol{n}_{i+1}\Delta\lambda\,\mathrm{d}V = \boldsymbol{N}_*\boldsymbol{e}_*\,, \tag{35}$$

$$\boldsymbol{N}_* = \int_V \boldsymbol{S}^t\boldsymbol{n}_{i+1}\boldsymbol{E}_*\,\mathrm{d}V, \tag{36}$$

$$\boldsymbol{N}_* = \left[\boldsymbol{S}^t(\boldsymbol{x}_1)\boldsymbol{n}_{i+1}(\boldsymbol{\sigma}(\boldsymbol{x}_1)),\quad \boldsymbol{S}^t(\boldsymbol{x}_2)\boldsymbol{n}_{i+1}(\boldsymbol{\sigma}(\boldsymbol{x}_2)),\quad \ldots,\quad \boldsymbol{S}^t(\boldsymbol{x}_N)\boldsymbol{n}_{i+1}(\boldsymbol{\sigma}(\boldsymbol{x}_N))\right]. \tag{37}$$

The weak form (38) of the yield condition, written for the modes that are active at instant t_{i+1} and for approximation (12), leads to the finite element description (39)

$$\int_V \delta\Delta\lambda F(\boldsymbol{\sigma}_{i+1})\,\mathrm{d}V = 0. \tag{38}$$

$$\int_V \boldsymbol{E}_*^t F(\sigma_{i+1})\,\mathrm{d}V \quad = 0. \tag{39}$$

The following is the resulting expression for the finite element solving system at instant t_{i+1},

$$\begin{cases} \boldsymbol{F}\boldsymbol{X}_{i+1} - \boldsymbol{A}\boldsymbol{q}_{i+1} + \boldsymbol{N}_*\boldsymbol{e}_* = \boldsymbol{v}_{i+1} - \boldsymbol{e}_{p_i}\,, & \text{(40a)} \\ -\boldsymbol{A}^t\boldsymbol{X}_{i+1} = -\boldsymbol{Q}_{i+1}\,, & \text{(40b)} \\ \displaystyle\int_V \boldsymbol{E}_*^t F(\boldsymbol{\sigma}_{i+1})\,\mathrm{d}V = 0. & \text{(40c)} \end{cases}$$

System (40) is non-linear due to Eq. (40c). This equation assumes that the set of active collocation points, $F(\boldsymbol{\sigma}_{i+1}(\boldsymbol{x}_k)) = 0$, is known at instant t_{i+1}. The inactive points, for which $F(\boldsymbol{\sigma}_{i+1}(\boldsymbol{x}_k)) < 0$, are not represented in system (40). The selection of the active and inactive control points at each step of the elastoplastic analysis is discussed in Section 4.4.

4.2. Linearisation

The non-linear system (40) can be recast in the residual form (41) and linearised by the Newton–Raphson Method, to yield, for each iteration j, the solving system (42),

$$\begin{cases} \boldsymbol{R}_1(\boldsymbol{X}_{i+1}, \boldsymbol{q}_{i+1}, \boldsymbol{e}_*) = \boldsymbol{F}\boldsymbol{X}_{i+1} - \boldsymbol{A}\boldsymbol{q}_{i+1} + \boldsymbol{N}_*\boldsymbol{e}_* - \boldsymbol{v}_{i+1} + \boldsymbol{e}_{p_i}, & (41a) \\ \boldsymbol{R}_2(\boldsymbol{X}_{i+1}, \boldsymbol{q}_{i+1}) = -\boldsymbol{A}^t\boldsymbol{X}_{i+1} + \boldsymbol{Q}_{i+1}, & (41b) \\ \boldsymbol{R}_3(\boldsymbol{X}_{i+1}) = \displaystyle\int_V \boldsymbol{E}_*^t F(\boldsymbol{\sigma}_{i+1})\, \mathrm{d}V, & (41c) \end{cases}$$

$$\begin{bmatrix} \boldsymbol{F} + \boldsymbol{M}_*^j & -\boldsymbol{A} & \boldsymbol{N}_*^{tj} \\ & 0 & 0 \\ \text{Symmetric} & & 0 \end{bmatrix} \begin{Bmatrix} \Delta\boldsymbol{X}^j \\ \Delta\boldsymbol{q}^j \\ \Delta\boldsymbol{e}_*^j \end{Bmatrix} = \begin{Bmatrix} \boldsymbol{R}_1 \\ \boldsymbol{R}_2 \\ \boldsymbol{R}_3 \end{Bmatrix}. \quad \begin{matrix} (42a) \\ (42b) \\ (42c) \end{matrix}$$

The following definitions are used in systems (41) and (42), respectively,

$$\boldsymbol{e}_{p_i} = \sum_{k=1}^{N} (\boldsymbol{S}^t\boldsymbol{\varepsilon}_{pi}), \tag{43}$$

$$\boldsymbol{M}_* = \int_V \boldsymbol{S}^t\nabla^2 F(\boldsymbol{\sigma}_{i+1})\boldsymbol{S}\boldsymbol{E}_*\boldsymbol{e}_*\, \mathrm{d}V = \sum_{k=1}^{N} \left[\boldsymbol{S}^t(\boldsymbol{x}_k)\nabla^2 F(\boldsymbol{\sigma}_{i+1}(\boldsymbol{x}_k))\boldsymbol{S}(\boldsymbol{x}_k)\Delta\lambda(\boldsymbol{x}_k)\right]. \tag{44}$$

System (42) is symmetric and highly sparse. Matrices $\boldsymbol{M}_*$ and $\boldsymbol{N}_*$ as well as vector $\boldsymbol{e}_p$ collect information on the so-called active collocation points $\boldsymbol{x}_k$. The iterative search method used to identify this set of points is presented in Section 4.4.

According to approximations (11) and (13) and to the elasticity condition (6), the stresses, displacements and elastic strains are defined at instant t_{i+1} by the following expressions,

$$\boldsymbol{\sigma}_{i+1} = \boldsymbol{S}\boldsymbol{X}_{i+1}, \tag{45}$$

$$\boldsymbol{u}_{i+1} = \boldsymbol{Z}\boldsymbol{q}_{i+1}, \tag{46}$$

$$\boldsymbol{\varepsilon}^e_{i+1} = \boldsymbol{f}\boldsymbol{S}\boldsymbol{X}_{i+1}. \tag{47}$$

4.3. Load step

The alternative method for controlling the load step proposed in [11] is adopted here. It consists in accepting variable load and displacement increments by controlling directly a prescribed increment of the external work. In the system (41), definition (29) for the load vector $\boldsymbol{Q}_{i+1}$ is replaced by the expressions below, where $\boldsymbol{t}_{\Gamma,\text{final}}$ is an (arbitrary) final load, and α_{i+1} is an unknown positive scalar,

$$\boldsymbol{Q}_{i+1} = \alpha_{i+1}\boldsymbol{Q}_T, \tag{48}$$

$$\boldsymbol{Q}_T = \int_{\Gamma_\sigma} \boldsymbol{Z}^t\boldsymbol{t}_{\Gamma,\text{final}}\, \mathrm{d}\Gamma. \tag{49}$$

The external work (50) at instant t_{i+1} is defined by Eq. (51) for the finite element approximation (13),

$$W_{i+1} = W_i + \Delta W = \int_{\Gamma_\sigma} \boldsymbol{t}^t_{\Gamma,\text{final}}\, \boldsymbol{u}_{i+1}\, \mathrm{d}\Gamma, \tag{50}$$

$$W_{i+1} = W_i + \Delta W = \int_{\Gamma_\sigma} \boldsymbol{t}^t_{\Gamma,\text{final}}\, \boldsymbol{Z}\boldsymbol{q}_{i+1}\, \mathrm{d}\Gamma. \tag{51}$$

Consequently, Eq. (41b) is replaced by result (52) and the additional residual (53) is added to system (41),

$$\boldsymbol{R}_2(\boldsymbol{X}_{i+1}\,,\,\boldsymbol{q}_{i+1}\,,\,\alpha_{i+1}) = -\boldsymbol{A}^t\boldsymbol{X}_{i+1} + \alpha_{i+1}\boldsymbol{Q}_T\,, \tag{52}$$

$$R_4(\boldsymbol{q}_{i+1}) = \boldsymbol{Q}_T^t\boldsymbol{q}_{i+1} - W_{i+1}\,. \tag{53}$$

The control parameter used in the incremental procedure implemented here, ΔW, is identified with a fraction of the external work spent in the elastic phase. The linear system (42) is extended to accommodate the additional scalar equation (53) needed to determine the load parameter, α,

$$\begin{bmatrix} \boldsymbol{F}+\boldsymbol{M}_*^j & -\boldsymbol{A} & \boldsymbol{N}_*^{tj} & 0 \\ & \boldsymbol{0} & \boldsymbol{0} & \boldsymbol{Q}_T \\ \text{Symmetric} & & \boldsymbol{0} & 0 \\ & & & 0 \end{bmatrix} \begin{Bmatrix} \Delta\boldsymbol{X}^j \\ \Delta\boldsymbol{q}^j \\ \Delta\boldsymbol{e}_*^j \\ \Delta\alpha_{i+1}^j \end{Bmatrix} = \begin{Bmatrix} \boldsymbol{R}_1 \\ \boldsymbol{R}_2 \\ \boldsymbol{R}_3 \\ R_4 \end{Bmatrix}. \tag{54a-d}$$

4.4. Solution procedure

Sub-matrices $\boldsymbol{F}$ and $\boldsymbol{A}$ present in system (54) are calculated just once, as they depend only on the elastic constants and the geometry of the elements. The number of columns of matrix $\boldsymbol{N}_*^t$, that is, the dimension of array $\Delta\boldsymbol{e}_*$, is variable as its depends on the number of active collocation points at the end of each the time step, which is not known in advance. The so-called Active Point Method is the strategy used here to solve this indeterminacy.

In this method, a collocation point $\boldsymbol{x}_k$ is said to be active if $F(\boldsymbol{\sigma}_{i+1}(\boldsymbol{x}_k)) \geq 0$. After implementing a set of iterations, the number of active points stabilises and the asymptotic quadratic convergence of the Newton–Raphson Method is regained. In the first iteration, the collocation points which were active at the end of the previous time step are assumed to remain active. When the Newton–Raphson process converges, the plasticity conditions are satisfied at all collocations points. Convergence occurs when $\Delta\boldsymbol{X}_i^j$, $\Delta\boldsymbol{q}$ and $\Delta\boldsymbol{e}_*$ are small enough and there are no collocation points where the plastic yield and flow laws are violated.

An alternative to the Active Point Method is the Active Set Method, frequently used also in Nonlinear Programming. In this method a set of active points is assumed and the Newton–Raphson method is applied and, after convergence, the set of active points is updated. The points that became active, $F(\boldsymbol{\sigma}_{i+1}(\boldsymbol{x}_k)) \geq 0$, during the process are accepted and those points that ceased being active, $\Delta\boldsymbol{e}_* < 0$, are removed from the set. The Newton–Raphson method is then restarted until the active set is stabilised.

In terms of the overall number of iterations, the Active Point Method has proved better than the Active Set Method in the tests reported in [4]. At each time step $[t_i\,,\,t_{i+1}]$ the initial estimate of the solution is taken as the vector $\{\boldsymbol{X}_i\,,\,\boldsymbol{q}_i\,,\,\boldsymbol{0}\}^t$. It means that the stress and displacement distributions are taken from the previous load step while assuming the plastic strains to be null.

The solving system (54) has variable dimensions and must be dynamically allocated in each iteration. It can be solved by Gauss elimination, taking into account its symmetry and sparsity, or by an iterative method, namely the pre-conditioned Conjugate Gradient Method. The option followed here is the Gauss elimination algorithm supported by a sparse storage scheme and a symbolic pre-factorisation analysis designed to minimise fill-in.

It is noted that, for large-scale problems, the combination of parallel solvers with the pre-conditioned Conjugate Gradient Method is the best solution scheme for system (54) [6]. This system is particularly well suited to parallel processing because the generalised stresses, $\boldsymbol{X}$, and the plastic multipliers, $\boldsymbol{e}_*$, are strictly element dependent, while the generalised boundary displacements, $\boldsymbol{q}$, are shared at most by two connecting elements.

5. NUMERICAL APPLICATIONS

A clamped cube and a tensile notched plate are used to test the application of the three-dimensional hybrid-Trefftz stress element. The results presented below are directly extracted from the references mentioned below or estimated from the graphs there presented when tabulated values are not available.

Different degrees in the approximation basis (11)–(13) are used in the implementation of the hybrid-Trefftz stress element. They are labelled HTS(d_σ , $d_{u\Gamma}$, N_p) in each test, where d_σ and $d_{u\Gamma}$ are the degrees used in the stress and boundary displacement approximations, respectively, and N_p defines the number of collocation points in each direction. Therefore, the total number of collocation points in each element is $(N_p)^3$.

The solutions presented for the hybrid-Trefftz stress element are those directly computed from approximations (11)–(13); no smoothing is used. A perfect plastic behaviour, with the Von Mises yield criterion and yield stress Y, is assumed in all tests.

The basic system of equations (1)–(10) is implemented in a non-dimensional form, which results from the application of three global scaling parameters, namely the length scale, L_s , the stress scale, Y_s , and the Young modulus scale, E_s , which are identified as the largest values found for these parameters in each application. Thus, the scaled values that replace the actual tractions and displacements are the following: $\lambda = t/Y_s$ and $\delta = uE_s/L_sY_s$.

5.1. Cantilever tests

The first set of tests is implemented on the clamped cube subject to a uniform transverse load, q, shown in Fig. 1. Symmetry is used to solve the cube with the four- and nine-element meshes defined in the same figure. The scaling parameters are $L_s = L$, $Y_s = Y$ and $E_s = E$ and the Poisson ratio used is $\nu = 0.3$.

Three sets of hybrid-Trefftz stress elements is used in each mesh, namely HTS(6,3,4), HTS(6,3,6) and HTS(4,2,4). The convergence of the corresponding load–displacement diagrams is presented in Figs. 2 and 3. The displacements measured is the vertical displacement at point A. As expected, p-refinement is more sensitive in the four-element mesh than in the nine-element mesh. The results obtained show, also, that p-refinement increases the collapse load while N_p-refinement induces lower collapse loads, as expected.

The HTS solutions are compared in Fig. 4 and in Table 1 with the solutions obtained with the 20-node C3D20 element available in the library of code ABAQUS [1]. This element is implemented using two regular meshes, with $4 \times 4 \times 4$ and $8 \times 8 \times 8$ elements. These solutions are compared also with the solutions obtained with two-dimensional stress models of the hybrid-Trefftz and hybrid-

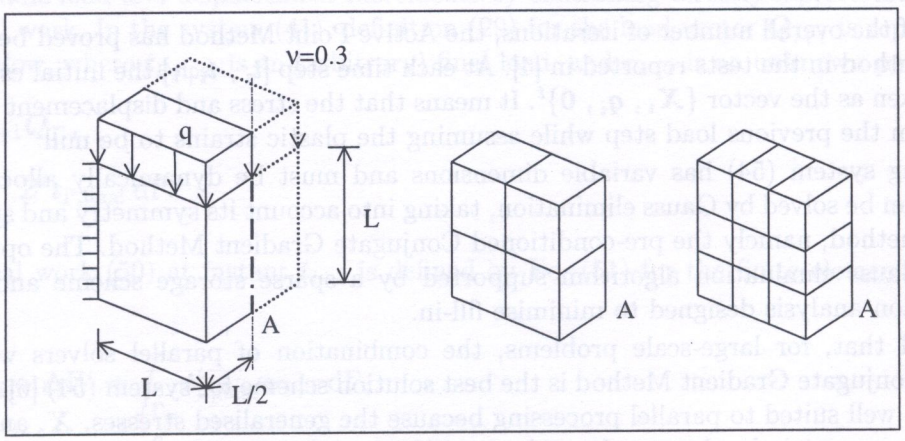

Fig. 1. Elastoplastic analysis of a clamped cube ($\nu = 0.3$)

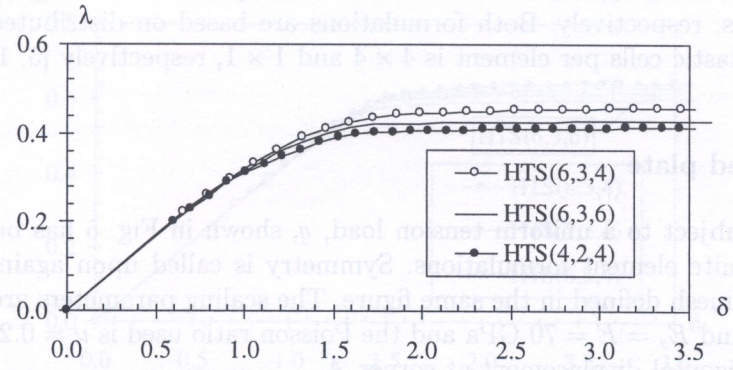

Fig. 2. Load–displacement diagrams for the clamped cube (4-element mesh)

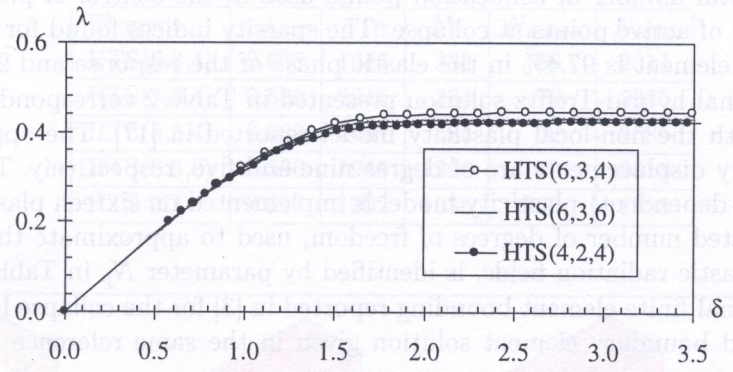

Fig. 3. Load–displacement diagrams for the clamped cube (9-element mesh)

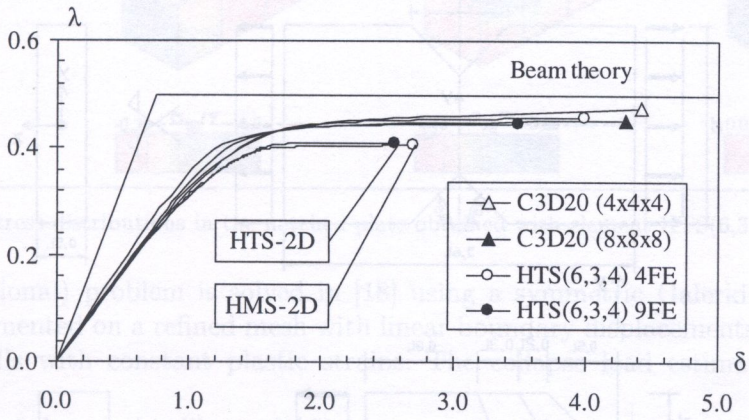

Fig. 4. Load–displacement diagrams for the clamped cube

Table 1. Collapse load estimates of the clamped cube at $\delta = 2.5$

Element	HTS-2D	HMS-2D	HTS(6,3,4)	HTS(6,3,4)	C3D20	C3D20
Mesh	4×4	32×32	4	9	$4 \times 4 \times 4$	$8 \times 8 \times 8$
λ_c	0.411	0.406	0.444	0.451	0.456	0.446

mixed finite element formulations, HTS-2D and HMS-2D, implemented on regular meshes with 4×4 and 32×32 elements, respectively. Both formulations are based on distributed plasticity models and the number of plastic cells per element is 4×4 and 1×1, respectively [5, 17].

5.2. Tensile notched plate

The notched plate subject to a uniform tension load, q, shown in Fig. 5 has been frequently used to test alternative finite element formulations. Symmetry is called upon again to solve the plate with the six-element mesh defined in the same figure. The scaling parameters are $L_s = L = 10$ mm, $Y_s = Y = 243$ MPa and $E_s = E = 70$ GPa and the Poisson ratio used is $\nu = 0.2$. The displacement considered is the horizontal displacement at corner A.

Four elements are tested, namely, HTS(8,3,4), HTS(7,3,4), HTS(6,3,4) and HTS(6,3,6). The corresponding load–displacement diagrams are shown in Fig. 6. The collapse load estimates are presented in Table 2, where N_{FE} defines the stress and boundary displacement degrees of freedom, N_P represents the total number of collocation points used in the control of plasticity and N_{actives} identifies the number of active points at collapse. The sparsity indices found for the Hessian matrix with the HTS(6,3,4) element is 97.4% in the elastic phase of the response and 97.2% at collapse.

The two-dimensional hybrid-Trefftz solution presented in Table 2 corresponds to the 20-element solution obtained with the non-local plasticity model reported in [17]. The approximation on the stresses and boundary displacements are of degree nine and five, respectively. The distributed and regularised (gradient-dependent) plasticity model is implemented on sixteen plastic cells per critical element. The associated number of degrees of freedom, used to approximate the plastic multiplier and the boundary plastic radiation fields, is identified by parameter N_p in Table 2.

The two-dimensional finite element bounding reported in [3] for the collapse load is $0.595 \leq \lambda_c \leq 0.625$ and the refined boundary element solution given in the same reference is $\lambda_c = 0.605$. The

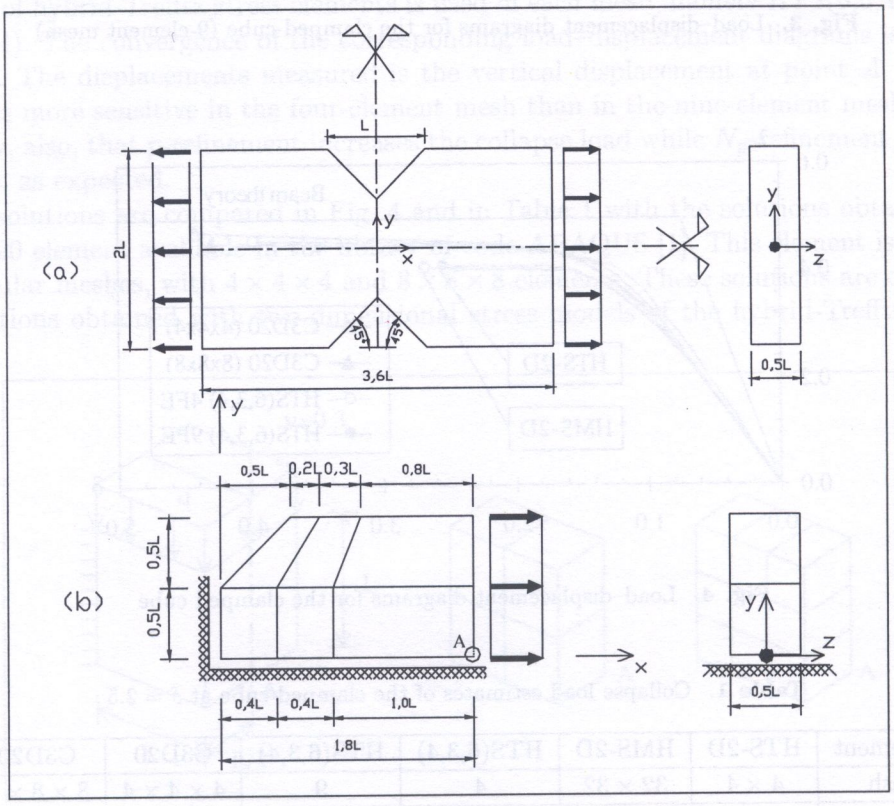

Fig. 5. Tensile notched plate ($\nu = 0.2$)

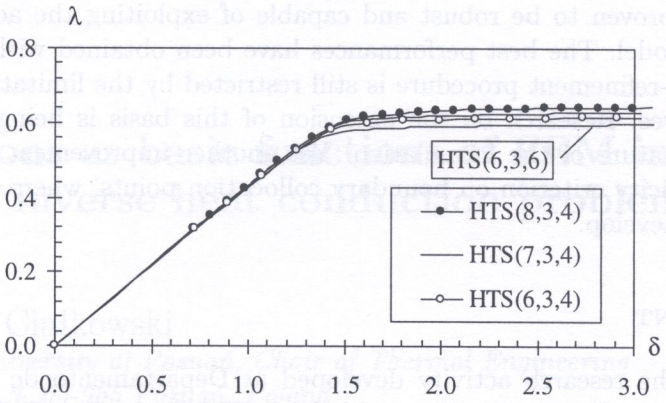

Fig. 6. Load–displacement diagrams for the tensile notched plate

Table 2. Collapse load estimates for the tensile notched plate at $\delta = 2.0$

Element	λ_c	N_{FE}	N_{P}	N_{active}	N_{total}
HTS(6,3,4)	0.608	1945	384	66	2011
HTS(7,3,4)	0.620	2215	384	70	2285
HTS(8,3,4)	0.632	2497	384	92	2589
HTS(6,3,6)	0.590	1945	1296	70	2015
HTS-2D	0.596	1302	1536	296	1598

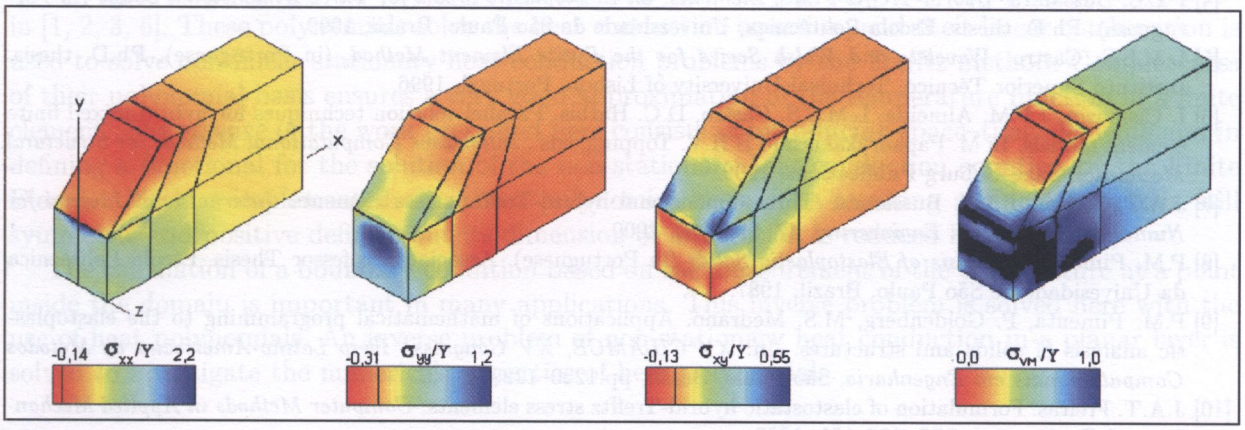

Fig. 7. Stress distributions in the notched plate obtained with element HTS(6,3,4) at $\delta = 2.0$

same (two-dimensional) problem is solved in [18] using a symmetric Galerkin boundary element formulation implemented on a refined mesh with linear boundary displacements, constant tractions, and triangular cells with constant plastic strains. The collapse load estimate reported there is $\lambda_c = 0.596$.

An adaptation of the graphic library [2] has been used to obtain the in-plane stress fields shown in Fig. 7. The equivalent Von Mises stress is shown also. The areas where the plastic criterion is corrupted ($\sigma_{vm}/Y \geq 1$) are printed in black. This local deterioration of the yield condition can be minimised simply by placing the plasticity control points on the surface of the elements.

6. Closure

The results reported above illustrate well the efficiency of the stress model of the hybrid-Trefftz stress finite element formulation in the solution of three-dimensional elastoplastic problems. The

algorithms used have proven to be robust and capable of exploiting the accuracy offered by the hybrid-Trefftz stress model. The best performances have been obtained with elements HTS(6,3,4) and HTS(7,3,4). The p-refinement procedure is still restricted by the limitation on complete stress basis of the sixth degree. Research on the extension of this basis is being developed to exploit fully the hierarchical nature of the formulation. Yet another improvement of the model consists in controlling the plasticity criterion on boundary collocation points, where the highest Von Mises stresses are known to develop.

ACKNOWLEDGEMENT

This work is part of the research activity developed at Departamento de Engenharia de Estruturas e Fundações, Escola Politécnica, Universidade de São Paulo, Brazil, Divisão de Engenharia Civil, Instituto de Pesquisas Tecnológicas do Estado de São Paulo, Brazil, and ICIST, Instituto Superior Técnico, Lisbon. It has been partially supported by FCT, Ministry of Science and Technology, Portugal, through research contract PRAXIS/2/2.1/CEG/33/94, and by CAPES, Ministry of Education, Brazil.

REFERENCES

[1] *ABAQUS Standard, Version 5.7.* Hibbit, Karlsson & Sorensen, Inc., 1997.

[2] J.P.M. Almeida. *Janela: Uma Interface Gráfica Destinada a aplicações de Mecânica Computacional*, versão preliminar. Instituto Superior Técnico, 1992.

[3] C.A. Brebbia, J.C.F. Telles, J.C.F., L.C. Wrobel. *Boundary Element Techniques*, Springer-Verlag, Berlin, 1984.

[4] F.L.S. Bussamra. *Hybrid-Trefftz Finite Elements: an Elastoplastic Model for Three-Dimensional Solids* (in Portuguese). Ph.D. thesis. Escola Politécnica, Universidade de São Paulo, Brazil, 1999.

[5] L.M.S.S. Castro. *Wavelets and Walsh Series for the Finite Element Method*, (in Portuguese). Ph.D. thesis. Instituto Superior Técnico, Technical University of Lisbon, Portugal, 1996.

[6] I. Cismasiu, J.P.M. Almeida, L.M.S.S. Castro, D.C. Harbis. Parallel solution techniques for hybrid-mixed finite element models. In M. Papadrakakis and B.H.V. Topping, eds., *Innovative Computational Methods for Structural Mechanics*, Saxe-Coburg Publications, 1999.

[7] J.A.T. Freitas, F.L.S. Bussamra. Three-dimensional hybrid-Trefftz stress elements. *International Journal for Numerical Methods in Engineering*, **47**: 927–950, 2000.

[8] P.M. Pimenta. *Analysis of Elastoplastic Solids* (in Portuguese). Associate Professor Thesis. Escola Politécnica da Univesidade de São Paulo, Brazil, 1987.

[9] P.M. Pimenta, P. Goldenberg, M.S. Medrano. Applications of mathematical programming to the elastoplastic analysis of solids and structures. In: *XV CILAMCE, XV Congresso Ibero Latino-Americano de Métodos Computacionais em Engenharia*, São Paulo, Brazil, pp.1220–1229, 1993.

[10] J.A.T. Freitas. Formulation of elastostatic hybrid-Trefftz stress elements. *Computer Methods in Applied Mechanics and Engineering*, **153**: 127–151, 1998.

[11] J.A.T. Freitas, J.P.M. Almeida, F.B.E. Virtuoso. Nonlinear analysis of space trusses. *Meccanica*, **20**: 144–150, 1985.

[12] J.A.T. Freitas, J.P.M. Almeida, E.M.B.R. Pereira. Non-conventional formulations for the finite element method. *Computational Mechanics*, **23**: 420–429, 1999.

[13] J.A.T. Freitas, C. Cismasiu. Numerical implementation of hybrid-Trefftz displacement elements. *Computers and Structures*, **4**: 1–19, 1999.

[14] J.A.T. Freitas, C. Cismasiu, Z.M. Wang. Comparative analysis of hybrid-Trefftz stress and displacement elements. *Archives of Computer Methods in Engineering*, **6**: 35–59, 1999.

[15] J.A.T. Freitas, Z.Y. Ji. Hybrid-Trefftz boundary integral formulation for the simulation of singular stress fields. *International Journal for Numerical Methods in Engineering*, **39**: 281–308, 1996.

[16] J.A.T. Freitas, Z.Y. Ji. Hybrid-Trefftz equilibrium model for crack problems. *International Journal for Numerical Methods in Engineering*, **39**: 569–584, 1996.

[17] J.A.T. Freitas, Z.M. Wang. Hybrid-Trefftz elements for elastoplasticity. *International Journal for Numerical Methods in Engineering*, **43**: 655–683, 1998.

[18] G. Maier, S. Miccoli, G. Novati, U. Perego. Symmetric Galerkin boundary element method in plasticity and gradient plasticity. *Computational Mechanics*, **16**: 1–15, 1995.